Fabrication and Structural Characteristics of Nanocrystalline Fe–Pt Thin Films and Fe–Pt Nanowire Arrays Embedded in Alumina Films on ITO/Glass

ARTICLE *in* THE JOURNAL OF PHYSICAL CHEMISTRY B · APRIL 2004

Impact Factor: 3.3 · DOI: 10.1021/jp0378642

4 AUTHORS, INCLUDING:

Song-Zhu Kure-Chu
Iwate University
48 PUBLICATIONS **1,262** CITATIONS

SEE PROFILE

Fabrication and Structural Characteristics of Nanocrystalline Fe−Pt Thin Films and Fe−Pt Nanowire Arrays Embedded in Alumina Films on ITO/Glass

Song-Zhu Chu,* Satoru Inoue, Kenji Wada, and Keiji Kurashima

Advanced Materials Laboratory, National Institute for Materials Science (NIMS), Namiki 1-1, Tsukuba, Ibaraki, 305-0044, Japan

Received: December 14, 2003; In Final Form: March 1, 2004

We described a new method to fabricate Fe−Pt binary alloy nanomaterials (nanocrystalline thin films and nanowire arrays embedded in porous alumina films) through a direct current electrodeposition in a novel bath with a simple composition on a glass substrate covered with a tin-doped indium oxide (ITO) film. The morphology and compositions of the Fe−Pt alloy films/nanowires are investigated by FESEM with an EDX analyzer, and the crystallographic structures of the two Fe−Pt nanomaterials were determined by XRD and HRTEM. Uniform Fe−Pt alloy films with bright appearance and controllable compositions in 14−90 atom % Fe were achieved on copper and ITO/glass within a broad current density range from 20 to 400 A/m^2. The Fe−Pt nanowires ($\phi \approx 50$ nm) embedded in anodic alumina films on ITO/glass were dense and parallel, with a high pore-filling of ≈95%, giving a high wire density of $\approx 4.7 \times 10^{14}$ wire/m^2. In particular, the Fe−Pt films and nanowires with a composition close to 1:1 Fe/Pt were polycrystalline with crystal sizes of 15−20 nm (films) and 3−6 nm (wires) across, which were identified to be cubic (Pt, Fe) phase with a lattice constant $a = 3.816$ Å.

Introduction

Fe−Pt binary alloys, especially chemically ordered $L1_0$ FePt with face-centered tetragonal (fct) structure, are important materials in permanent magnetic applications, because of their large uniaxial magnetocrystalline anisotropy ($K_u = 6.6 \times 10^6$ J/m^3), satisfied mechanical strength, and good chemical stability.[1,2] Conventional investigations on Fe−Pt magnetic films were mainly conducted using vacuum deposition techniques such as sputtering and vapor deposition,[3−7] in which Fe−Pt alloy films was deposited as multilayered structures and then annealed to produce ordered phases. The magnetic properties such as coercivity and easy axis of magnetization of the Fe−Pt alloy films are usually parallel to the film plane due to the planar structures. Recently, several studies reported a new method to fabricate monodisperse FePt nanoparticles by colloid synthesis techniques.[8−12] When prepared in self-organized two- and three-dimensional arrays and annealed at appropriate temperature, the monodisperse FePt nanoparticles with a fct structure developed enhanced coercivities, though little difference between in-plane and out-of-plane coercivities and hysteresis behavior was found due to the random orientation of the individual FePt nanoparticles.

Electrodeposition is a well-known surface-finishing technology and is usually used to acquire various alloy films or coatings on metallic substrates (e. g., carbon steels) for anticorrosion, antiabrasion, and other physical and chemical properties.[13] Electrodeposition is usually advantageous over other "dry" coating technologies due to its low cost, simple equipment, and large-scale processing. So far, a variety of Fe (Co, Ni)-based alloys in thin films or nanowires have been electrodeposited in many studies for magnetic applications.[14−20] While electrodeposition of Fe−Pt alloys[20] has been rarely investigated, because of a technical difficulty in the codeposition of iron and platinum with their significant potential difference. In particular, finding a stable and reproducible electrolyte system (bath) is essential for achieving Fe−Pt alloys with controllable compositions and performance, and this has not been done well yet. In the present study, we report the fabrication of nanocrystalline Fe−Pt alloys on ITO/glass substrates by a direct current electrodeposition in a novel bath with a simple composition. Particularly, we attempt a novel process to fabricate Fe−Pt nanowire arrays directly on glass substrates, which may have potential applications in ultrahigh density perpendicular magnetic recording media due to the predicted enhanced perpendicular coercivity of nanowires relative to other Fe−Pt materials.

Experimental Section

Fabrication of Fe−Pt Alloy Films. Electrodeposition of Fe−Pt alloys was carried out in a constant current mode (5−600 A/m^2, 1−6 V) in an acidic bath containing 0.5 M $FeSO_4$, 0.02 M $FeCl_2$, 7.7 mM H_2PtCl_6, and 50 ppm $CH_3(CH_2)_{11}OSO_3$-Na, at 25 °C and pH = 2.0−3.0, with vigorous mechanical stirring. The low pH value and room temperature were adopted to prevent the precipitation of $Fe(OH)_2$ (pH > 3). The electrolyte system (bath) and electrodeposition conditions were determined by a series of preliminary experiments with a 247-mL Hull cell on copper plates.

A glass plate (soda lime, 25 × 100 × 0.7 mm) coated with a tin-doped indium oxide (ITO: ≈120 nm, ≈10 Ω/□) film was used as the working electrode to fabricate Fe−Pt alloy films on it. In experiments, the ITO-covered glass was first ultrasonically cleaned in acetone for 10 min, immersed in diluted H_2SO_4 solution (≈1%) for 2−3 s, and finally rinsed with distilled water. A platinum plate (30 × 120 × 2 mm) was used as the counter electrode. The distance between the working electrodes and the counter electrode is fixed at 2 cm.

* To whom correspondence should be addressed. Phone: +81 29 851 3354 (ext 8600). Fax: +81 29 854 9060. E-mail: CHU.Songzhu@nims.go.jp.

10.1021/jp0378642 CCC: $27.50
Published on Web 04/14/2004

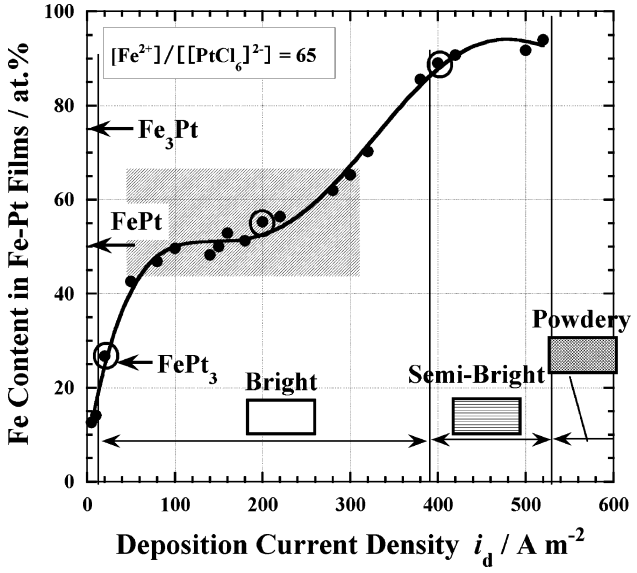

Figure 1. Effect of deposition discrepancy current density (i_d) on composition of Fe−Pt alloy films on copper plates. (pH = 2.4, T_d = 25 °C, t_d = 10 min.). The schematic insets show the appearance of the specimens.

Fabrication of Fe−Pt Nanowire Arrays. The fabrication procedure of the nanowires is similar to our previous studies.[19,21] In simple terms, a highly pure aluminum layer (99.99%, ≈1.5 μm) was first deposited by RF-sputtering on the ITO-covered glass substrate as described before. The specimens were then anodized in a 3 wt % oxalic acid solution at 40 V and 10 °C, until the Al metal was completely converted into alumina. The porous anodic alumina films ($\phi \approx 50$ nm) on ITO/glass, after the removal of the insulative barrier layer (5% H_3PO_4, 30 °C, 15 min), were used as template electrodes in a dc electrodeposition to deposit Fe−Pt alloys within the nanopores. The applied current density associated with the apparent areas for electrodeposition of Fe−Pt nanowires was calculated according to the porosity of the porous anodic alumina films (≈0.38) and the values determined by the Hull-cell test, which was designated to be 40−120 A/m^2 to achieve an Fe−Pt alloy close to 1:1 atomic ratio (see the later description). During the anodization and electrodeposition, the variations of current and voltage were monitored by two multimeters connected with a programmed computer system.

Characterizations. The morphologies of the specimens were observed by a field emission scanning electron microscope (FESEM) (S-5000, Hitachi). To minimize charging effects, the specimens were covered with a thin evaporated 0.4−0.6 nm osmium film. The compositions of Fe−Pt alloys were determined by the energy-dispersive X-rays analyzer (EDX) equipped on the FESEM. The crystallographic structures of Fe−Pt thin films and nanowires were investigated by an X-ray diffractometer (XRD) (RINT-2200V/PC, Cu Kα, 40 kV/40 mA) and a transmission electron microscope (TEM) (JEM-2020, 200 kV). For TEM observation, the Fe−Pt film or the Fe−Pt wires/Al_2O_3 composite layer were first scratched off from the ITO/glass substrates and smashed and then set on carbon-coated copper microgrids and observed in a bright field.

Results and Discussion

Influence of Deposition Current Density on Compositions of Fe−Pt Alloy Films. Controlling the alloy composition of electrodeposited films is essential to the crystallographic structure and properties of the films. Figure 1 shows the effect of deposition current density on the composition of Fe−Pt alloy films on copper plates. Under the given conditions, the Fe content in the Fe−Pt alloy films increases with the current density (i.e., codeposition potential), varying in a broad range from 14 to 94 atom % at current densities of 10−600 A/m^2. This is consistent with the behavior of normal codeposition in alloy electrodeposition and allows the adjustment of the composition in Fe−Pt films through deposition current density.

The electrodeposition behavior (or composition variation) of Fe−Pt alloys can be mainly ascribed to the potential difference of iron and platinum ions, which may exist in Fe^{2+} and $[PtCl_6]^{2-}$ in the electrolyte. During electrodeposition, the Fe^{2+} ions and $[PtCl_6]^{2-}$ complex ions may be reduced through the following electrochemical reactions:[22]

$$Fe^{2+} + 2e^- = Fe \quad E^0_1 = -0.403 \text{ V (vs SHE)} \qquad (1)$$

$$[PtCl_6]^{2-} + 2e^- = [PtCl_4]^{2-} + 2Cl^- \quad E^0_2 = +0.720 \text{ V (vs SHE)} \qquad (2)$$

$$[PtCl_4]^{2-} + 2e^- = Pt + 4Cl^- \quad E^0_3 = +0.730 \text{ V (vs SHE)} \qquad (3)$$

The large potential difference ($\Delta E^0 = (E^0_2 + E^0_3) - E^0_1 = 1.853$ V), which usually relates to a large depositing potential difference, may mainly contribute to the significant dependence of alloy composition on current density or deposition potential. As the cathodic current density increases, the deposition potential of platinum may become much more negative, due to a strong cathodic polarization, thus decreasing the depositing potential difference between iron and platinum and leading to the increasing of iron content in Fe−Pt films. Moreover, the dissociation rate of $[PtCl_6]^{2-}$ complex ions and the difference of transportation rate or mobility between $[PtCl_6]^{2-}$/$[PtCl_4]^{2-}$ complex ions and Fe^{2+} ions driven by the electrical field may delay the supply of $[PtCl_4]^{2-}$ complex ions on the electrode. That is, the deposition of platinum is mainly governed by mass transport kinetics and the iron deposition mainly by reaction kinetics, thus leading to the increase of the iron component with increasing cathodic current density. It was also found in our preliminary experiments that changing the concentration and concentration ratio of Fe^{2+} and $[PtCl_6]^{2-}$ ions resulted in little effect on the composition of alloy films, indicating a predominate dependence on potential difference or current density.

In addition, it should be noticed that the atom %−i_d curve exhibits a "platform" at 50−250 A/m^2, with a narrow composition range of 45−55 atom % Fe, which is just situated in the formation range of the γ_3 (FePt) phase (hatched region, 45−67 atom %Fe).[23] This is advantageous to achieve a uniform composition distribution in electrodeposited Fe−Pt alloy films and to maintain the crystallographic phase uniformity, especially for electrodes with indefinite areas, e.g., porous anodic alumina films on ITO/glass as described later.

Appearance and Microstructures of Fe−Pt Alloy Films on Copper. The deposition current density also affects the appearance and/or morphology of Fe−Pt alloy films. Figure 1 also illustrates the appearance of the electrodeposited Fe−Pt alloy films as evaluated by the naked eye. Uniform and continuous Fe−Pt alloy films with typical metallic luster were formed within a broad i_d range from 10 to 520 A/m^2 (mirror bright appearance at 10−400 A/m^2 and semibright appearance at 400−520 A/m^2), indicating a good leveling performance of the electrolyte system. This enables us to form various Fe−Pt alloy films with different compositions and necessary mechan-

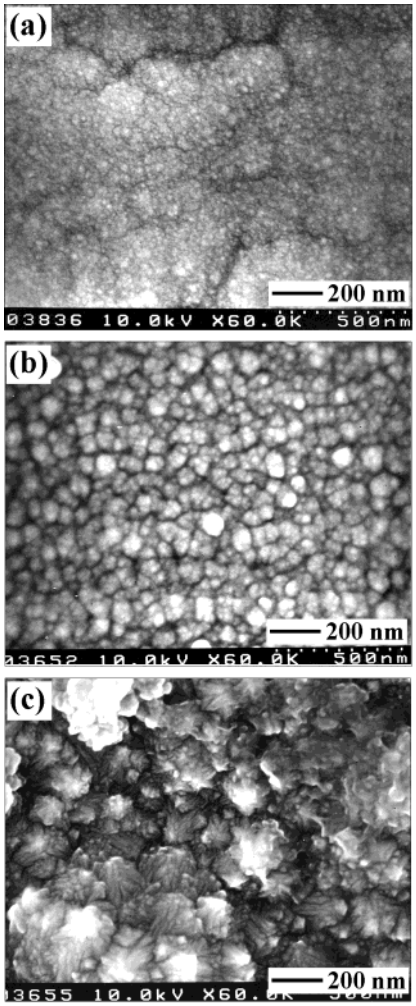

Figure 2. Field-emission scanning electron microscopic (FESEM) images of surface morphologies of as-electrodeposited Fe−Pt alloy films on copper plates obtained at different current densities of (a) 20 A/m^2 ($Fe_{27}Pt_{73}$), (b) 200 A/m^2 ($Fe_{55}Pt_{45}$), and (c) 400 A/m^2 ($Fe_{89}Pt_{11}$).

ical strength for many applications. Electrodeposition at high current densities over 520 A/m^2 caused violent gas (hydrogen) evolution and led to discontinuous or powdery Fe−Pt films with poor adherence to the copper substrate, possibly due to the high stress developed in the alloy films.

Figure 2 shows the representative FESEM images of the surface morphology of Fe−Pt alloy films on copper obtained at different current densities (see circles in Figure 1). At lower current density (Figure 2a, 20 A/m^2), the deposited film is fine and smooth, indicating the formation of small grains at lower deposition rate. At moderate current density (Figure 2b, 200 A/m^2), the Fe−Pt films are still uniform and smooth, but the grain size increases to some extent, indicating that the high deposition rate promotes the grain coagulation or crystal growth in Fe−Pt alloy films. Finally, at high current density (Figure 2c, 400 A/m^2), a coarse Fe−Pt film with large grains and a semibright metallic luster is obtained, possibly due to the high deposition rate and/or the formation of Fe-rich crystals. Moreover, it was also found that powdery Fe−Pt deposits with numerous nodules were formed at current densities over 520 A/m^2 (not shown), possibly due to the high Fe content in alloy films that leads to lower corrosion resistance.

Electrodeposition of Fe−Pt Alloy Films on ITO/glass. Uniform Fe−Pt alloy films with similar appearance to the films on copper can be obtained on bared ITO/glass, though higher deposition potentials than on copper are correspondingly needed for identical current densities, because of the relatively high resistance of the ITO film. Figure 3 gives the representative FESEM images of a thin Fe−Pt film formed on ITO/glass with an atomic ratio near 1:1. Compared to the identical film formed on copper substrate (Figure 2b), the Fe−Pt deposits on ITO/glass exhibit a similar morphology but are composed of large grains, even over a short deposition time (2 min; see arrows). Generally, the activation energy for nucleation on nonmetallic or oxide electrodes by electrodeposition is larger than on metallic ones due to the difference of the electronic affinity between metallic and nonmetallic substances. It could be deduced that the Fe−Pt nuclei formed on an ITO film in the initial stage of electrodeposition may be less than on a Cu plate, even when performed at the identical depositing current density. During electrodeposition, as soon as Fe−Pt nuclei formed, Fe−Pt deposition afterward may occur preferentially on the Fe−Pt nuclei instead of on ITO film, because the activation energy for crystal growth is usually smaller than that for nucleation, thus leading to the Fe−Pt deposits with relatively large grains. In addition, unlike copper substrate, continuous Fe−Pt films with elevated thickness were difficult to achieve on an ITO/glass substrate. It was found in experiments that a uniform, thin Fe−Pt film was first formed on the ITO/glass with a bright appearance (Figure 3b). While the deposition goes on, some cracks were produced, and the Fe−Pt film gradually disintegrated into a discontinuous film and even spontaneously peeled off from the ITO/glass substrate, possibly due to the weak adherence to the ITO film and/or the high stress of the as-electrodeposited alloy films.

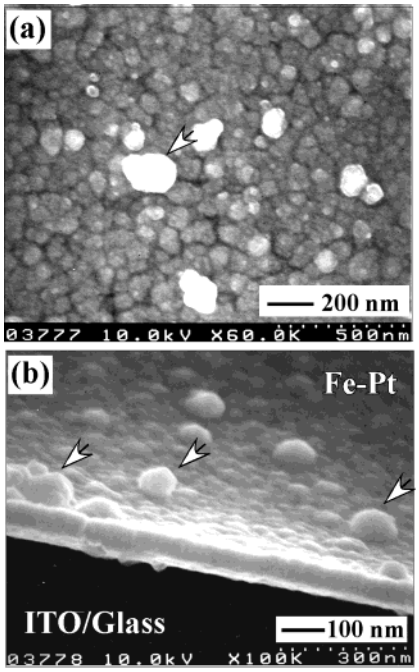

Figure 3. FESEM images of (a) surface morphology and (b) a fracture section of an Fe−Pt alloy film on ITO/glass (200 A/m^2, $Fe_{48}Pt_{52}$).

Fabrication of Fe−Pt Nanowire Arrays in Porous Alumina Films on ITO/Glass. On basis of the electrodeposition method of continuous Fe−Pt alloy films, a through-template electroplating was attempted to fabricate Fe−Pt nanowire arrays in porous alumina films, which are formed by anodization of a pure aluminum layer sputter-deposited on ITO/glass.[19,21,24] To get Fe−Pt alloys with uniform compositions close to the chemically ordered FePt phase, electrodeposition for Fe−Pt nanowires was performed at an overall current density of 80 A/m^2 related to the apparent areas of the specimens, to get Fe−

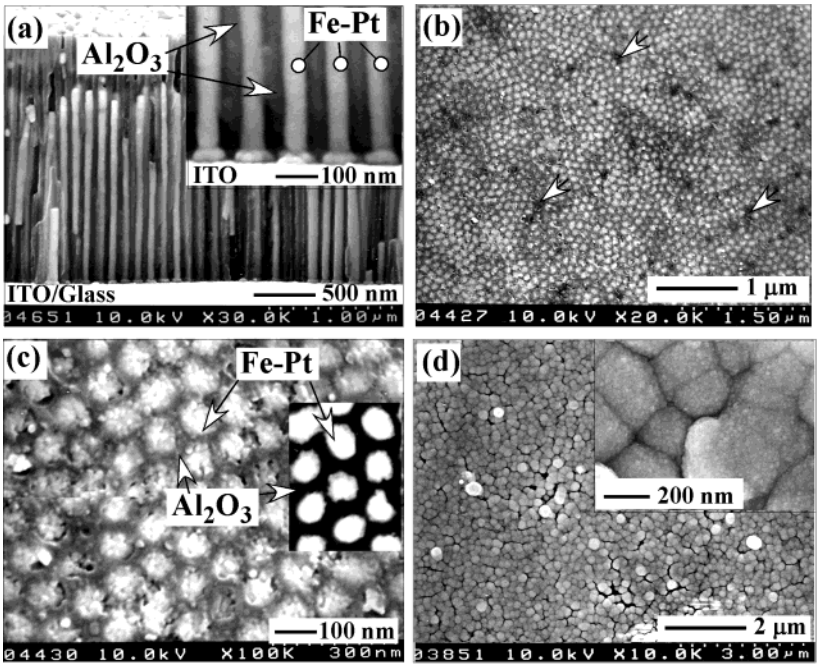

Figure 4. FESEM images of (a) the vertical fracture section, (b, c) bottom views of Fe−Pt nanowire arrays embedded in anodic alumina films on ITO/glass, and (d) surface morphology of an overfilled Fe−Pt film on porous alumina. The inset in c is a backscattering electron image (BSI) image.

Pt nanowires that are a little Fe-rich. At the beginning of the electrodeposition, the transparent template electrode with porous alumina films became nearly uniformly black, indicating the filling of Fe−Pt electrodeposits in porous alumina films. After depositing for several minutes, the Fe−Pt deposited up to the top of the pores and then overfilled on alumina films on ITO/glass. In case of overfilling, a continuous Fe−Pt film with bright appearance formed on the alumina films.

Figure 4 shows the FESEM images of Fe−Pt nanowire arrays embedded in anodic alumina films on ITO/glass. The Fe−Pt alloy nanowires filled densely and uniformly in the pores of the alumina films on ITO/glass substrate, with a smooth surface and nearly uniform diameter upright (Figure 4a), which reflect the contour of the porous alumina template. In the present study, the average diameter and the cell size (pore interspacing) for as-anodized alumina films are $\phi \approx 30$ and 100 nm, respectively, and the average diameter and wire interspace of the Fe−Pt alloy nanowire array are both ≈50 nm after chemical dissolution and electrodeposition (inset in Figure 4a), thus leading to an ordered composite nanostructure with periodical magnetic and nonmagnetic materials. The height or length of the nanowires in the pores is dependent on depositing time. In the case where the full thickness of the anodic alumina films (≈2.1 μm) is completely filled with Fe−Pt alloys, the aspect ratio of the nanowires is ≈42. Moreover, the images of surface morphology (Figure 4b,c) reveal that more than 95% of the pores of the alumina film are uniformly filled with Fe−Pt nanowires, indicating the good filling and wetting ability of the electrolyte system. Here, the filling of the pores may be further improved by ultrasonic stirring, and the highly ordered arrangement of the nanowires may be achieved by a preindentation process when necessary.[25] In addition, the density of nanowires, i.e., nanopores of anodic alumina films, can be readily controlled through the anodizing voltages and electrolytes, with higher pore density in lower voltage.[19,21] In the present study, the density of the FePt nanowires is calculated to be $\approx 4.7 \times 10^{14}$ wire/m^2.

An overfilled Fe−Pt continuous film on anodic alumina is also shown in Figure 4d. The overfilled Fe−Pt film (≈300 nm) is composed of larger grains with finer and smoother morphology (see inset in 4d) than the identical films on copper and bared ITO/glass (Figures 2b and 3a), which could be ascribed to the induction from the pores of anodic alumina films through the "electrical filter" (porous alumina) during the overfilling electrodeposition. More importantly, the overfilled Fe−Pt films (300 nm-3 μm) on alumina exhibited very good adhesion in a tear-off test compared to the films formed on bared ITO/glass, which can be ascribed to the "anchor" effect of the nanowires that inserted in porous alumina films.

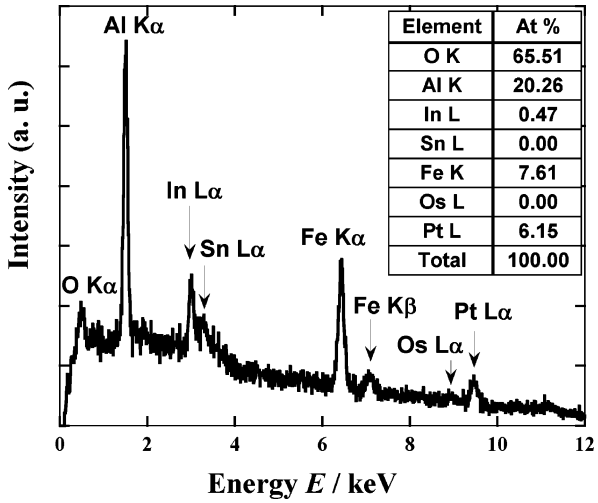

Element	At %
O K	65.51
Al K	20.26
In L	0.47
Sn L	0.00
Fe K	7.61
Os L	0.00
Pt L	6.15
Total	100.00

Figure 5. A typical EDX spectrum of an Fe−Pt alloy nanowire array embedded in an alumina film on ITO/glass (see FESEM image in Figure 4b). The inserted table shows the corresponding integrated concentrations.

Figure 5 gives a typical energy-dispersive X-ray spectrum of the Fe−Pt/alumina/ITO/glass specimen shown in Figure 4a. The Fe Kα and Pt Lα peaks are clearly seen, which confirms the codeposition of Fe and Pt elements by electrodeposition. The Al Kα and O Kα peaks are attributed to the porous anodic alumina film and the In Lα peak to the underlying ITO film on glass substrate, due to the thinness of the composite Fe−Pt/

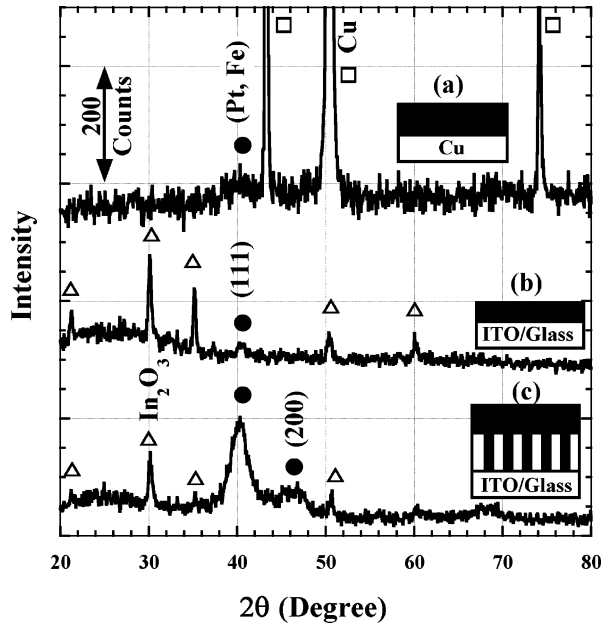

Figure 6. X-ray diffraction patterns of (a) an $Fe_{55}Pt_{45}$ film on copper, (b) an $Fe_{48}Pt_{52}$ film on ITO/glass, and (c) an $Fe_{51}Pt_{49}$ nanowire array embedded in an anodic alumina film on ITO/glass.

alumina layer. The corresponding integrated concentration of the composite layer is also given as an inset in Figure 5. The average composition for the resultant Fe−Pt nanowires is calculated to be 51 atom % Fe−49 atom % Pt, close to the desired composition of 1:1 atomic ratio, which is consistent with the Fe−Pt alloy films obtained at the identical current density on copper and bared ITO/glass (Figures 2b and 3).

Crystallographic Structures of Fe−Pt Alloys. The phase compositions of as-electrodeposited alloy films have a great deal to do with the performance of the films in many aspects. The crystallographic structures of as-electrodeposited Fe−Pt alloy films and nanowires are investigated by X-ray diffraction analysis and transmission electron microscopy, as shown in Figures 6 and 7. The Fe−Pt alloy films obtained on copper (Figure 6a) and on bared ITO/glass (Figure 6b) only show a faint hump near 40.4°, which could either infer an amorphous structure or be ascribed to the thinness of the Fe−Pt alloy films (Figure 3b). The composite Fe−Pt nanowires/alumina layer on ITO/glass (Figure 6c) exhibits two broad peaks at 40.38° and 46.5°, inferring a microcrystal structure.

Figure 7 demonstrates the TEM images of a continuous $Fe_{48}Pt_{52}$ film and an $Fe_{51}Pt_{49}$ nanowire array inserted in porous alumina. Numerous tiny grains or crystals are clearly seen in the high-resolution images (Figure 7a,c), and the corresponding selected area electron diffraction patterns (insets a′ and b′) exhibit several continuous rings, indicating the polycrystalline structures for both Fe−Pt alloys. According to calculations, the rings in the SAED patterns are close to those of (111), (200), (220), and (311) reflections of cubic (Pt, Fe) phase with a lattice constant $a = 3.816$ Å (Card No.29-0718). This confirms that the as-electrodeposited Fe−Pt alloys, whether as thin film or nanowires, are polycrystalline and composed of tiny crystals. In particular, the crystal size for the continuous Fe−Pt film (15−20 nm across, Figure 7a) is 3−5 times larger than that for the Fe−Pt nanowires (3−6 nm across, Figure 7c), indicating that the Fe−Pt electrodeposits tend to form larger grains on a planar electrode, i.e., the bared ITO/glass without dimensional restriction, than on a nanoporous electrode, i.e., porous alumina-covered ITO/glass with confinement of the pores in the transverse direction. Moreover, the relatively slow ion transportation through the porous alumina films during electrodeposition may also partly contribute to the formation of small Fe−Pt crystals.

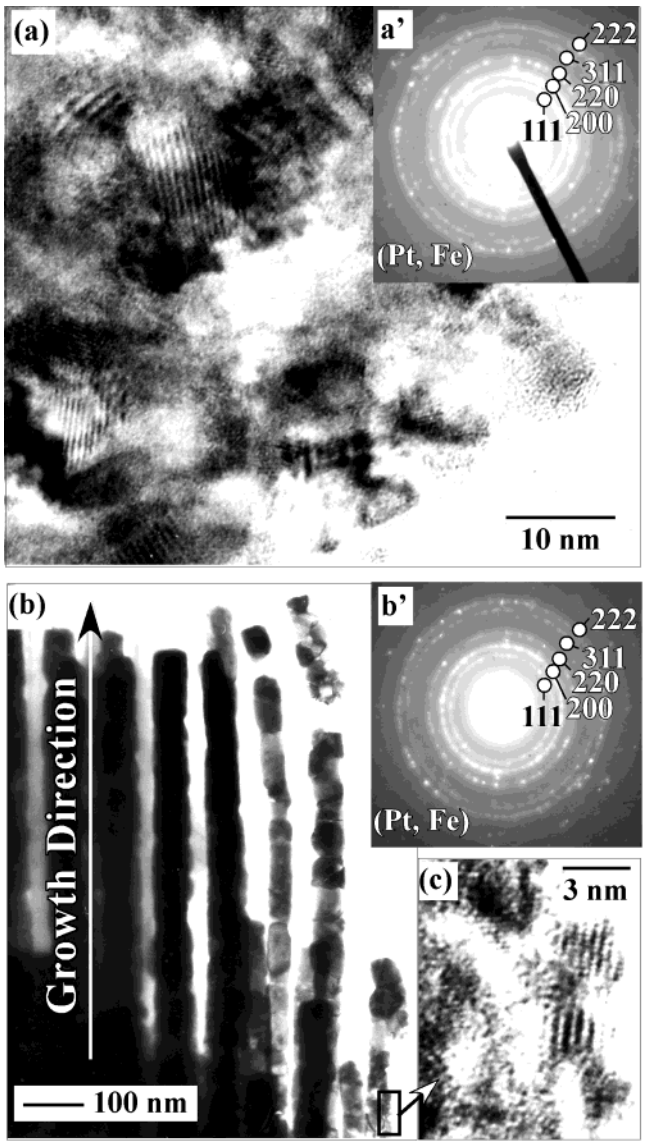

Figure 7. Transmission electron microscopic (TEM) images of (a) an $Fe_{48}Pt_{52}$ alloy film and (b, c) $Fe_{51}Pt_{49}$ nanowires partly embedded in an anodic alumina film. Insets a′ and b′ are the corresponding electron diffraction patterns of a and b, respectively.

In addition, according to the calculation from the Scherrer formula ($0.9\lambda/\beta \cos \theta$, where β = fwhm of the (111) plane, $\lambda = 1.5405$ Å), the average size of the crystallites for the Fe−Pt film/wires (Figure 6c) is approximately estimated as ≈10 nm, possibly reflecting the crystal size of the overfilled Fe−Pt film on porous alumina films. The crystal size of the overfilled Fe−Pt layer is just between those of Fe−Pt nanowires and the continuous Fe−Pt film, indicating that the pores of alumina films also affect the growth of Fe−Pt crystals through the "electrical filter" (i.e., porous alumina) during overfilling electrodeposition.

Conclusions

We fabricated successfully Fe−Pt alloy films and nanowires with controllable compositions on copper and ITO/glass substrates by using electrodeposition in a new, stable, and feasible bath. We also presented a novel process to fabricate reproducibly high-density ($\approx 4.7 \times 10^{14}$ wire/m^2) and narrow ($\phi \approx 50$ nm) Fe−Pt (≈1:1) alloy nanowire arrays in porous anodic alumina

films on ITO/glass substrates, which may endow a promising application as ultrahigh density perpendicular magnetic recording media, due to the predictable enhanced perpendicular magnetic performance after appropriate annealing. Moreover, even though we concentrated on fabrication of single-layered Fe−Pt films and single-composition Fe−Pt nanowires in the present paper, the potential impact of our approach may be much broader. For instance, our electrolyte system may be used to fabricate multilayered Fe−Pt alloy films[26] and multilayered nanowires with different compositions by adjusting current density periodically or by pulsed electrodeposition, which are being explored.

Acknowledgment. This work is part of the Japan Millennium Project of Exploration and Creation of a Catalyst for Removing Harmful Chemical Substances.

References and Notes

(1) Skomski, R.; Coey, J. M. D. *Permanent Magnetism*; Institute of Physics Publishing: Philadelphia, 1999, p 269.

(2) Sellmyer, D. V. *Nature* **2002**, *420*, 374.

(3) Weller, D.; Moser, A.; Folks, L.; Best, M. E.; Lee, W.; Toney, M. F.; Schwichert, M.; Thiele, J.-U.; Doerner, M. F. *IEEE Trans. Magn.* **2000**, *36*, 10.

(4) Ristau, R. A.; Barmak, K.; Lewis, L. H.; Coffey, K. R.; Howard, J. K. *J. Appl. Phys.* **1999**, *86*, 4527.

(5) Liu, J. P.; Luo, C. P.; Liu, Y.; Sellmyer, D. J. *Appl. Phys. Lett*. **1998**, *72* (4), 483.

(6) Ping, D. H.; Ohnuma, M.; Hono, K.; Watanabe, M.; Iwasa, T.; Masumoto, T. *J. Appl. Phys.* **2001**, *90*, 4708.

(7) Huang, Y.; Okumura, H.; Hadjipanayis, G. C.; Weller, D. *J. Magn. Magn. Mater.* **2002**, *242*−*245*, 317.

(8) Sun, S.; Murray, C. B.; Weller, D.; Folks, L.; Moser, A. *Science* **2000**, *287*, 1989.

(9) Zeng, H.; Li, J.; Liu, J. P.; Wang, Z. L.; Sun, S. *Nature* **2002**, *420*, 395.

(10) Stahl, B.; Gajbhiye, N. S.; Wilde, G.; Kramer, D.; Ellrich, J.; Ghafari, M.; Hahn, H.; Gleiter, H.; Weissmüller, J.; Würschum, R.; Schlossmacher, P. *Adv. Mater.* **2002**, *14* (1), 24.

(11) Shevchenko, E.; Talapin, D.; Kornowski, A.; Wiekhorst, F.; Kötzler, J.; Haase, M.; Rogach, A.; Weller, H. *Adv. Mater.* **2002**, *14* (4), 287.

(12) Stahl, B.; Ellrich, J.; Theissmann, R.; Ghafari, M.; Bhattacharya, S.; Hahn, H.; Gajbhiye, N. S.; Kramer, D.; Viswanath, R. N.; Weissmüller, J.; Gleiter, H. *Phys. Rev. B* **2003**, *67*, 014422.

(13) Ukai, Y.; Kishi, M.; Tokunaga, M.; Mita, I. *Reviews of Surface Finishing Technology: A handbook For Electrodeposition and Anodization*; Kohshinsha Co. Ltd.: Tokyo, 1983, p 295.

(14) Schmid, G. *J. Mater. Chem.* **2002**, *12*, 1231.

(15) Thurn-Albrecht, T.; Schotter, J. G.; Kästle, A.; Emley, N.; Shibauchi, T.; Krusin-Elbaum, L.; Guarini, K.; Black, C. T.; Tuominen, M. T.; Russell, T. P. *Science* **2000**, *290*, 2126.

(16) Khan, H. R.; Petrikowski, K. *J. Magn. Magn. Mater.* **2002**, *249* (3), 458.

(17) Gadad, S.; Harris, T. M. *J. Electrochem. Soc.* **1998**, *145* (11), 3699.

(18) Tourillon, G.; Pontonnier, L.; Levy, J. P.; Langlais, V. *Electrochem. Solid State Lett.* **2000**, *3* (1), 20.

(19) Chu, S. Z.; Wada, K.; Inoue, S.; Todoroki, S.; Takahashi, Y. K.; Hono, K. *Chem. Mater.* **2002**, *14*, 4595.

(20) Huang, Y. H.; Okumura, H.; Hadjipanayis, G. C.; Weller, D. *J. Appl. Phys.* **2002**, *91* (10), 6869.

(21) Chu, S. Z.; Inoue, S.; Wada, K.; Hishita, S. *J. Electrochem. Soc.* **2004**, *151* (1), C38.

(22) Dobos, D. *Electrochemical Data: A handbook For Electrochemists in Industry and Universities*; Elservier Scientific: New York, 1975, p 260.

(23) Massalki, T. B. *Binary Alloy Phase Diagrams*, 2nd ed.; ASM International, Materials Park, OH, 1990; p 1755.

(24) Chu, S. Z.; Wada, K.; Inoue, S.; Todoroki, S. *J. Electrochem. Soc.* **2002**, *149* (7), B321.

(25) Masuda, H.; Yanagishita, T.; Yasui, K.; Nishio, K.; Yagi, I.; Rao, T. N.; Fujishima, A. *Adv. Mater.* **2001**, *13* (4), 247.

(26) Jyoko, Y.; Schwarzacher, W. *Electrochim. Acta* **2001**, *47*, 371.